공학석사학위논문

Fabrication and Characteristic Analysis of Direct Printed Graphene Oxide Based Supercapacitors

직접 인쇄된 그래핀 옥사이드 수퍼 커패시터의 제작 및 특성분석

2015 년 2월

서울대학교 대학원

기계항공공학부

치아창비

Fabrication and Characteristic Analysis of Direct Printed Graphene Oxide Based Supercapacitors

직접 인쇄된 그래핀 옥사이드 수퍼 커패시터의 제작 및 특성분석

Academic Advisor: Junghoon Lee

Submitting a master's thesis of engineering

January 2015

Graduate School of Seoul National University

Department of Mechanical and Aerospace Engineering

Cheah Chang Ve

Confirming the master's thesis written by Cheah Chang Ve

January 2015

Chair Mansoo Choi (Seal)

Vice Chair Junghoon Lee (Seal)

Examiner Seung Hwan Ko (Seal)

Abstract

Fabrication and Characteristic Analysis of Direct Printed Graphene Oxide Based Supercapacitors

Cheah Chang Ve

Department of Mechanical and Aerospace Engineering

Seoul National University

This thesis reports an innovative approach to fabricate flexible interdigitated supercapacitors via the combination of graphene oxide (GO) patterning with an ultra-low-volume liquid dispenser and GO photo-thermal reduction. GO solution is delivered on a specific surface to create a functional nanostructure with high porosity, leading to a "printed" electrical double layer capacitor or supercapacitor that demonstrates a high energy density. High flexibility in terms of architecture and substrate material makes this energy storage device favorable for intelligent power applications.

21st century sees the continual revolution in the IT world that incessantly alters human life style, especially through the invention of may smart devices. Along with this development, there are increasing needs for

electrical energy storage with high energy density that can meet the power demands of new smart circuits. For instance, energy harvesting for remote sensors requires supercapacitors fully integrated with on-chip circuitry. Bulky sandwich structure of a conventional supercapacitors are likely less effective in these applications. Alternative to that complicated structure, the use of porous material in interdigitated configuration on a substrate can be a feasible solution.

A low volume liquid handling instrument was employed in the printing process. It is programmable to deliver GO droplets onto a substrate to achieve a high resolution pattern. This essentially simplifies electrode patterning process because current collector components and masking procedures are avoided. In this manner, GO pattern was interdigitated on a PET film. Photothermal reduction approach was opted to recover the electrical properties of pristine graphene, using a commercial camera flash accessory. Optimization of flash reduction was of paramount importance to induce effective photothermal effect while maintain the integrity of the electrode structure. Through appropriate surface treatment and direct printing approach as well as optimized reduction conditions, supercapacitors can be realized on various substrates such as thin films and other device surfaces.

Device characterization was achieved through electrochemical means. Cyclic voltammetry, galvanostatic charging-discharging test,

electrochemical impedance spectroscopy and capacitance retention test were performed and detailed in performance analysis.

Keywords: Direct printing, Graphene oxide, Photothermal reduction, Electrical double layer capacitor, Supercapacitor

Student number: 2013-22487

Contents

List of Figures

List of Graphs and Tables

1. Introduction

1.1. Supercapacitor – An energy storage device

Energy storage devices are indispensable in today's world where we are surrounded by ever power-hungry electronics. Batteries have been the most prevalent choice since the last century. Despite superior capacity, secondary batteries such as lithium ion batteries still suffer from critical limitations that arise from the slow Faradaic process which they rely on[1]. Consequently, batteries are not only plagued by sluggish power performance, but their usage is also largely hindered by poor cyclability due to material degradation[2].

Several decades ago, people began to shift attention to supercapacitors that seemingly promising to fill the voids between electrolytic capacitor and battery. Supercapacitors or electrochemical capacitors are capable to tackle the aforementioned drawbacks of batteries. One hallmark of supercapacitors is their high charging and discharging rate [3, 4], usually falls in the range of seconds or minutes, depending on the capacity. Supercapacitors are extremely useful in terms of providing a surge of output energy in a short period of time. Such characteristic makes them irreplaceable and complementary with secondary batteries in many applications including automotive and wind energy generation systems. Another attractive features of supercapacitors is their excellent cyclic stability. They can operate more than 500 000 cycles without major

performance drop. Fast charging-discharging capability and highly stable cycle life are attributed to the non-faradaic charge storage mechanism, through the formation of electrical double layer on the electrode-electrolyte interphase. The general operating conditions of supercapacitors and batteries are compared and summarized in Table 1.

Supercapacitors are advantageous in high power oriented devices that need remarkable cycle life. Typically, supercapacitors are equipped in a wide range of high power delivery applications such as electric transportation, elevators, hand tools, flashlights, welding and defibrillator. They are also useful in energy harvesting systems where rapid charging ability is needed to store energy harvested from surroundings. Besides, supercapacitors find practical application in uninterruptable power supply (UPS) that replace electrolytic capacitors for cost effectiveness. Beyond bulky equipment, supercapacitors are also incorporated as main power source in tiny devices such as sensor platform, smart devices and implantable medical devices. More and more applications are being explored with the use of supercapacitors. Large demand in many diverse areas is driving the research and development of the energy storage device.

Table 1 Comparison of supercapacitors and batteries.[5]

Key Characteristic	Units	Supercapacitor	Batteries
Voltage	V	2.5-5	1.2-4.2
Operating temperature	℃	-40 to +70	-20 to +60
Cycle life		>500,000	300-10,000
Calendar life	Years	5-20	0.5-5
Energy density	Wh/L	1-10	100-300
Power density	W/L	1000-10,000	100-3,000
Efficiency	%	>98	70-95
Charge rate	C/x	>1500	<40
Discharge rate		Sec/Minutes	Hours

1.2. Development and current researches of supercapacitors

A capacitor is an electrical device used to store energy in electrostatic field using a pair of conductors or electrodes, sandwiching an insulating dielectric material. The invention of capacitor in 18th century came through with glass as the dielectric[6]. Energy storage is possible due to charge separation that creates a potential difference between the conductors. The magnitude of the stored energy relies on the dimension as well as material properties of the electrodes, and the electrical potential between the electrodes which is limited by the dielectric breakdown of the insulator.

Ceramic, film type and electrolytic capacitors are built based on identical concept. It is noteworthy that polarized electrolytic capacitors has relatively high capacitance. It contains either solid or liquid electrolyte that functions as cathode, while a thin metal oxide layer that grown on anode is the dielectric material where electrostatic field establishes. The energy storage mechanism is different from supercapacitors, in which charge storage takes place owing to electrical double layer or pseudocapacitance. The discussion of supercapacitor in the entire thesis is restricted only for electrical double layer capacitor (EDLC).

The working principle and structure of supercapacitor will be elaborated in following sections. Generally, supercapacitor utilizes carbon nanomaterials as electrodes for their large specific surface area and excellent electrical properties. Ruoff's group has proposed to use

chemically modified graphene (CMG) as electrode materials in a sandwich configuration[7]. Chemical binder was mixed with CMG particles to construct the electrodes. Other than sandwich configuration, planar configuration with interdigital pattern was also developed. MEMS fabrication provides well-established techniques to pattern such delicate current collectors and electrodes such as micro-supercapacitors based on monolithic carbide-derived carbon films[8]. Later on, ultra-high power micrometer-size supercapacitors were made using onion-like carbon as active material[3]. Onion-like carbon was electrophoretically deposited on interdigitated gold current collectors that were produced using conventional photolithography and etching process. Furthermore, numerous works were dedicated for simpler device structure and patterning process. Laser sources were used to simultaneously reduce graphene oxide and produce desirable interdigitated patterns. For instances, direct laser writing on hydrated graphite oxide films[9] and laser scribing using commercial DVD writer [4, 10]. Innovative supercapacitor fabrication approaches are also being reported like using soft lithography[11] and printing technologies[12].

2. Theoretical Background

2.1. Capacitance

The simplest capacitor can be constructed by putting two pieces of metal plate facing each other in close proximity, with an insulator held in between to avoid physical contact. During the charging process where the metal plates are connected to direct current power supply, current flows in the circuit. A charge Q will move from one plate to another, causing the plates to be charged with +Q at one side and equally magnitude of –Q at another. Charges accumulate on the metals until the potential between the plates balances the external potential. The plates or capacitor will remain charged even when the external power supply is removed, as how electrical energy is stored in the device. It is more accurate to say that energy is stored in the electrostatic field established between the plates. The electrostatic field grows stronger as current flows in, charging the device. On the other hand, the charges on the plates will be released and electrons start flowing in the circuit when an external load is connected, until the potential between the plates is neutralized. This is known as discharging process.

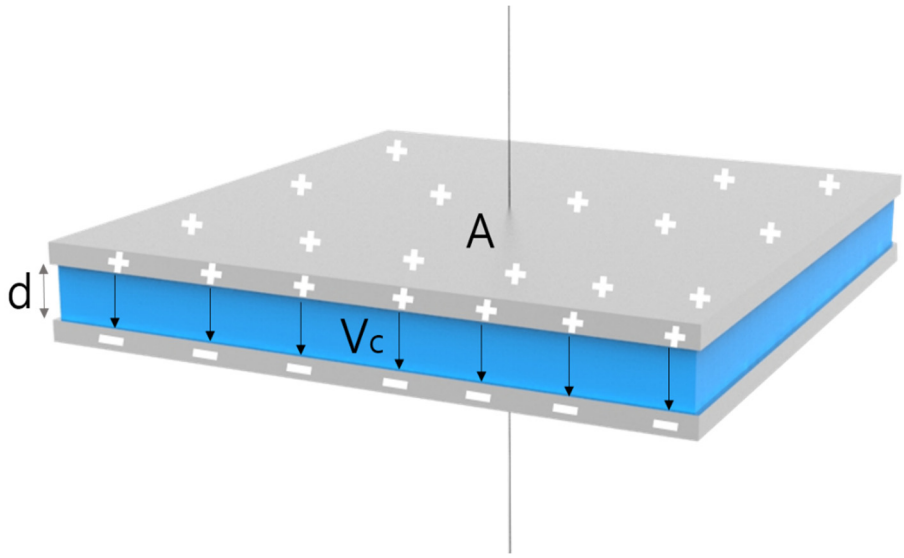

Figure 1 Parallel plate capacitor.

Capacitance is the electrical property that represents the ability of a capacitor to store electrical charge, in the unit of Farad (F). It can be defined as charge accumulated in the plates for a given unit potential difference (V).

$$C = \frac{Q}{V}$$

The capacitance of the device is proportional to the areal size of plate, A and dielectric constant of the insulating material, while inversely proportional to the distance between the plates, d. Capacitance can be expressed in following equation,

$$C = \frac{\varepsilon \kappa A}{d}$$

where ε is the permittivity of space and κ is dielectric constant of the insulating material.

Supercapacitors operate under exactly same principle while having much higher capacitance than electrolytic capacitor, swiftly exceeding 100 F. Such significant capacitance enlargement is mainly attributed to the electrode materials used in supercapacitor, which are mostly carbon based, instead of metal. Advance in nanotechnology has produced various carbon based nanomaterials which attains extremely high surface, such as fullerene, carbon nanotube, graphene, and activated carbon. High surface area electrodes are needed to hold additional charges on the electrode.

Nevertheless, supercapacitors do not use traditional dielectric materials like ceramic and thin polymer film to separate the electrodes. Instead when electrical potential is provided, the ions contained in electrolyte form an electrical double layer in the electrode-electrolyte interphase where solvent molecules stay in between the ions and the electrodes. (The structure and principle of double layer are articulated in the following 2.2 section.) This solvent molecules layer plays critical roles of the dielectric materials as in traditional capacitors. The key advantage offered by this double layer is the extraordinary short separation distance between the charged electrodes and the ions, which is within atomic length. This narrow gap is crucial because it reduces the electrical potential because the electric field between the parallel plates is constant.

$$E = \frac{V}{d}$$

Subsequently, more charge is needed to be loaded on the plate to maintain

the voltage, resulting in higher capacitance. Hence, the collective contributions from the large electrode surface area and short separation distance in double layer essentially expand the capacitance to the level unreachable by the traditional capacitors.

In the charging process, ions are attracted by Coulomb forces towards opposite charged porous electrodes, which leads to the formation of electrical double layer at both electrodes. Each double layer structure can be visualized as a capacitor. Thus, a symmetrical supercapacitor that consists of two identical electrodes can be considered as a combination of two capacitors connected in series, shown in Figure 2. During discharging process, electrons flows from one electrode to another through an external circuit. This removes the charges gathered on the electrodes and diminishes the Coulomb attraction acting on the ions at the interphase. Accordingly, ions desorb from the electrode surface. The discharging process is depicted in Figure 3.

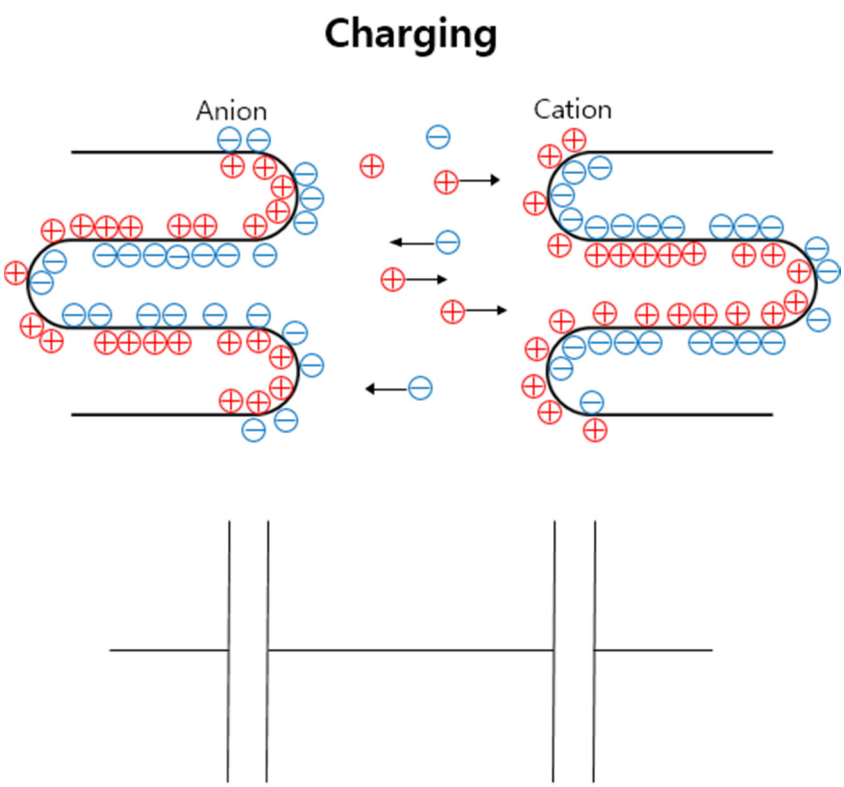

Figure 2 Charging process. Ions are absorbed on the porous electrode. Two electrical double layers behave as two capacitors connected in series.

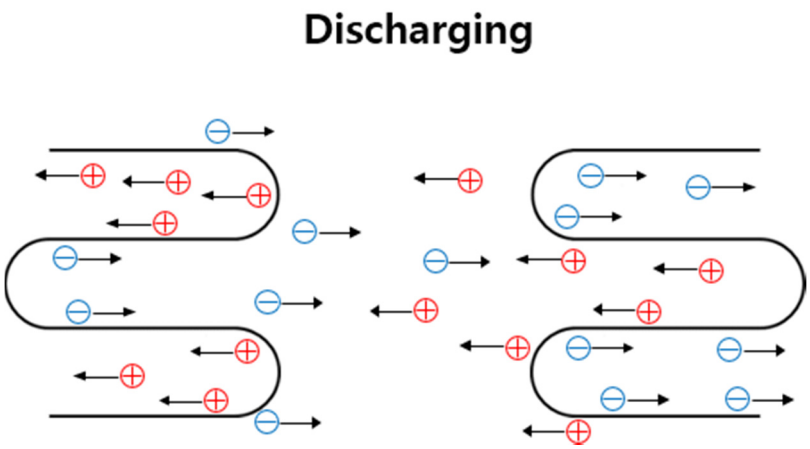

Figure 3 Discharging process. Ions are desorbed from the electrode surface and charge accumulated on both electrodes are released.

2.2. Electrical Double Layer

The capacitance of electrical double layer capacitor (EDLC) is resulted from the formation of a layer of counter ions on the electrode surface to form two array layers of opposite charges. The structure of such layers has been meticulously studied and argued since 1ate 19^{th} century when von Helmholtz first proposed the basic model of double layer. Helmholtz suggested the accumulation of a compact layer of ions that maintains a distance about 1nm from the electrode surface. This distance is considered as the layer thickness that depends on the ion size and the applied voltage.

Several decades later, it was clear that the compact ion layer cannot be static under the effects of thermal motion according to Boltzmann principle. A new model known as Gouy-Chapman, was then proposed in such way that the ions should be seen as point charges that float randomly in the electrolyte, which motion was explained with Poisson-Boltzmann equations. Thus, a diffuse ion layer extending into the electrolyte from the electrode surface was proposed. This model suffers from incorrect potential profile as well as over-large capacitance prediction owing to the point charge assumption. Gouy-Chapman model was corrected by Stern who had combined both Helmholtz and Gouy-Chapman models that consisted of a compact ion layer and diffuse layer.

Grahame developed further the double layer theory by distinguishing inner and outer layer of Helmholtz layer. Such distinction is because of the size difference between cations and anions. [13] Smaller cations are

surrounded by the solvent molecules due to the ion solvent dipole interactions, resulting in a larger dimension with the solvation shells. Since anion layer is located nearer to the electrode compared to the cation layer, usually the capacitance on positive electrode is higher than the negative electrode. Further from the electrode and double layer, there is a diffuse layer as well in Grahame's model.[14] The latest development of the double layer addressed the interaction between the dipolar solvent (water) and the electrode, because of excessively higher concentration of solvent than solute. [15]

The double layer formed at the electrode surface can be represented using a simple model shown in Figure 4. Inner Helmholtz plane (IHP) spans from the center of compact ion layer whereas outer Helmholtz plane (OHP) passes from the center of solvated ion to the electrode surface. Lastly, the diffuse layer covers from OHP onwards. The thickness of double layer is approximated at $1.5\kappa^{-1}$, where κ^{-1} is the Debye-Huckel length [16] which is given as

$$\kappa^{-1} = (\varepsilon_r \varepsilon_0 k_B T / 2c^0 z_i^2 e^2)^{1/2}$$

ε_r : Relative dielectric permittivity of solvent
ε_0 : Permitivity of vacuum
k_B : Boltzmann constant
T : Temperature
z : Ion charge
e : Electron charge

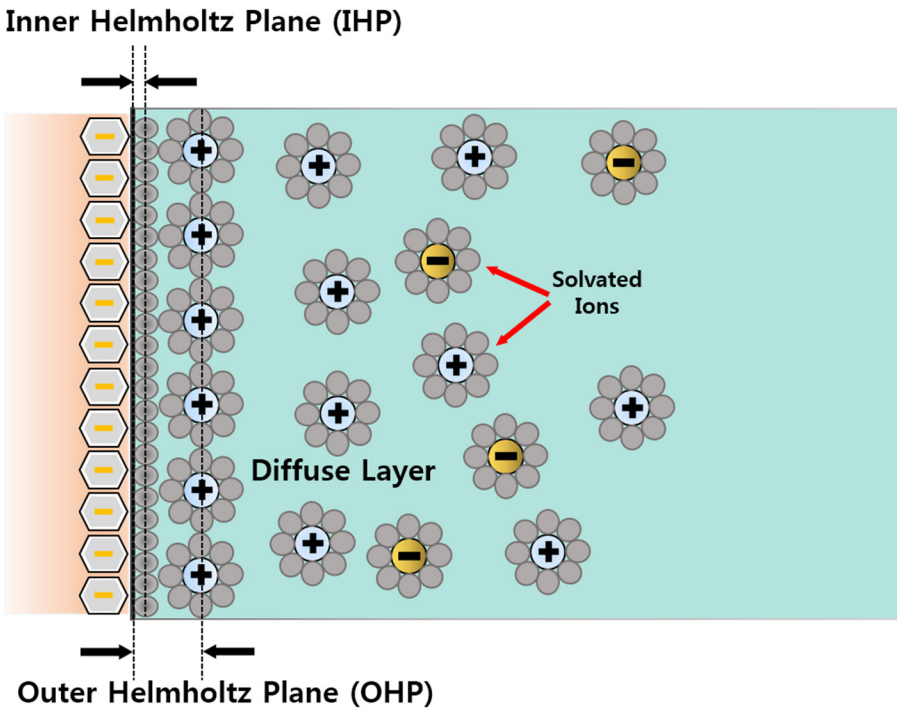

Figure 4 Structure of electrical double layer.[17]

3. Materials and Methods

3.1. Electrode material

Supercapacitors store electrical energy through the physical interaction between the ion species in the electrolyte and the electrodes that forms electrical double layer. It is intuitive that materials with high specific surface area can accommodate more ions, leading to larger capacity. In addition, supercapacitor electrode have to be electrically conductive, chemically and thermally stable to ensure low equivalent series resistance and long cycle life. Riding the tides of popularity in nanotechnology, many carbon nanomaterials such as fullerene, carbon nanotubes, graphene and activated carbon are produced in industries and laboratories and being tested in various applications. Particularly, these graphitic materials are also being investigated rigorously for supercapacitor applications [18-20].

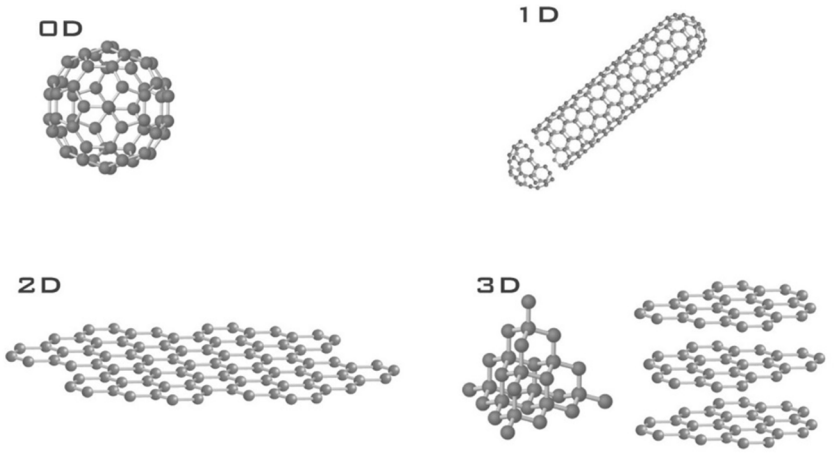

Figure 5 Carbon allotropes: Fullerene, carbon nanotube, graphene, diamond and graphite.[21]

Graphene, the building unit of graphite, is one-atom-thick carbon sheet that attains two dimensional forms. Graphene attracts massive attention because of its extraordinary mechanical properties, high specific surface area ($2600\ m^2/g$) and excellent electrical properties [22, 23]. It can be prepared through top-down or bottom-up approaches. Top-down approaches are referred to processes in which three dimensional graphite structure is exfoliated into two dimensional sheets, mechanically or chemically. Typical examples are micromechanical exfoliation using Scotch tape, creation of colloidal suspensions like graphene oxide, transversal cutting of carbon nanofiber and unzipping of carbon nanotubes. In contrast, bottom-up approaches rely on self-assemble of carbon sources in molecular level into larger and more complex structures, for instances, chemical vapor deposition (CVD) of hydrocarbon, epitaxial growth and organic synthesis.

Bottom-up approaches offer high quality graphene but usually require high temperature environment which may hinder its use in some applications. Graphene preparation through graphene oxide suspension is commonly used due to simplicity and high production yield. Graphite structure is exfoliated into layers through series of rigorous oxidation process, which is widely known as Hummer's method. Graphene oxide (GO) obtained needs to undergo reduction process to remove attached functional groups in order to recover electrical conductivity. GO used for electrode precursor material dispersed in water, has concentration of 5g/L and flake size in the range of 0.5 to 5 microns.

3.2. Pattern design

In general, the configuration of supercapacitors can be categorized into two groups: stacked type and planar type (Figure 6).

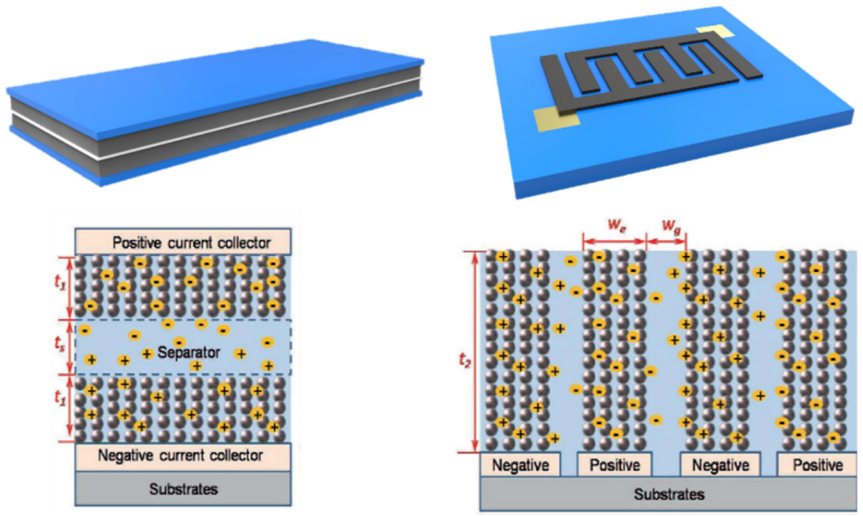

Figure 6 Stacked and planar configurations. Shorter ion diffusion length in planar geometry where ions rely on lateral movement.[23]

Stacked type is the kind which electrodes are stacked together, while a separator is sandwiched in between to prevent physical contact of the electrodes. This configuration enables more loading of electrode material to increase the total capacity of the energy storage device. Another possible configuration of supercapacitors is the planar geometry, in which the electrodes are built as interdigitated conformation on a same surface.

Planar geometry eliminates the use of separator which is the primary resistive force exerted on the ions in the migration process during charging and discharging. Swift movement of the ions leads to better power performance of the storage device. Moreover, the ion diffusion length is

shorter in interdigitated configuration than its counterpart. Ions mainly rely on lateral movements that they can get through the porous material more smoothly and quickly. In contrast to this, ions have to penetrate deeply into the porous electrode for empty spots, resulting in longer diffusion length in stacked type.[24]

Planar geometry was opted in this research. Both cathode and anode consist of four fingers interdigitating with each other, as shown in the figure below. The horizontal side was made up with 22 spots, while vertical was 25 spots. Taking into account the dispensing error, the dimension of the pattern was measured at 1750 μm × 1890 μm including the spacing between the fingers.

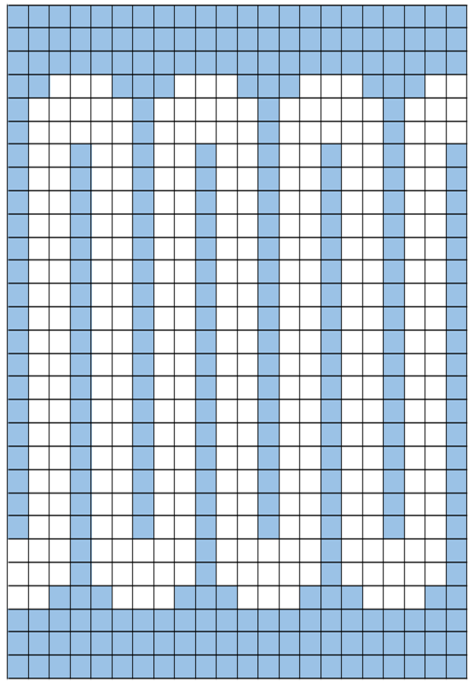

Figure 7 Printing layout

3.3. Printing procedures

GO can be viewed as graphene sheets with basal plane is decorated by oxygen-containing functional groups. These functional groups have high affinity to water molecules, making GO hydrophilic and dissolvable in water. The solubility of GO in water allows itself to be used as ink in the printing approach. A liquid dispenser (sciFLEXARRAYER DW, Scienion, Germany) is employed to deliver GO solution directly onto a flexible polyethylene terephthalate (PET) film. The piezoelectric-driven nozzle of the dispenser is able to eject solution of volume as low as 300 pL. The dispenser is programmed to jet out GO droplets at designated spot on the substrate to produce patterns (Figure 8).

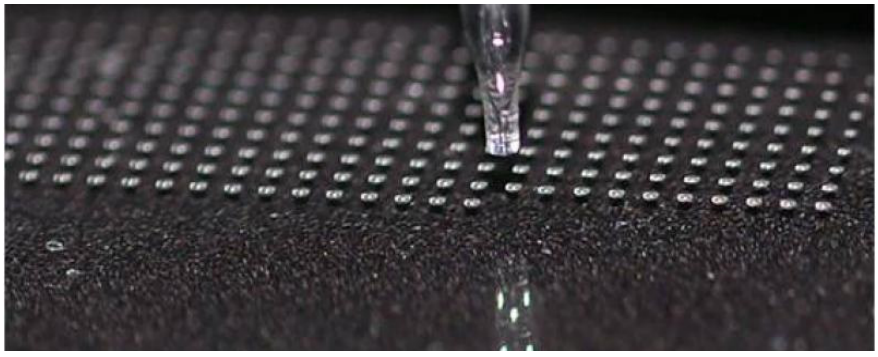

Figure 8 Ultra low volume dispensing.[25]

Prior to printing, PET surface was treated with high voltage using a Tesla coil to reduce the substrate surface energy, resulting in a more hydrophilic surface. It is crucial to control the surface energy to promote effective GO reduction and good adhesion after the reduction process. Due to stress

resulted from the volume expansion after reduction[26], reduced graphene oxide (rGO) are prone to delamination when the interfacial energy is high as reflected in large contact angle. It was observed that GO was more easily reduced when it was deposited on surface with higher contact angle. At higher contact angle, GO structure was thicker because droplet was focused onto smaller area of deposition. However when the interfacial energy is low as in the case of GO on glass surface, the photothermal reduction hardly took place. GO droplet formed a thin transparent layer on glass surface, which was not effective to capture photothermal energy.

The droplets were maintained at 80 μm from each other, an optimal distance to make a continuous line while effectively avoided coalescence of the droplets which are shown in Figure 10. Droplet coalescence should be avoided to prevent disconnection of printed lines as shown in Figure 9.Various patterns are possible; anode and cathode rGO lines were interdigitated to maximize charge storage area. The thickness of the printing pattern could be controlled through multiple layer dispensing, in which active material was stacked up layer by layer. Similar to 3D printing, new layer was added onto previously printed surface after the preceding layer dried out from evaporation. In this manner, ten layers of GO interdigitated pattern was printed before proceeding to reduction process. Figure 11 displays the printed pattern through multiple layer dispensing.

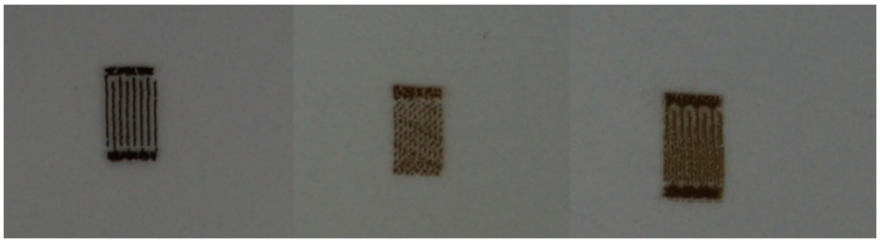

Figure 9 Printing failure. GO lines were not well connected due to droplet coalescence.

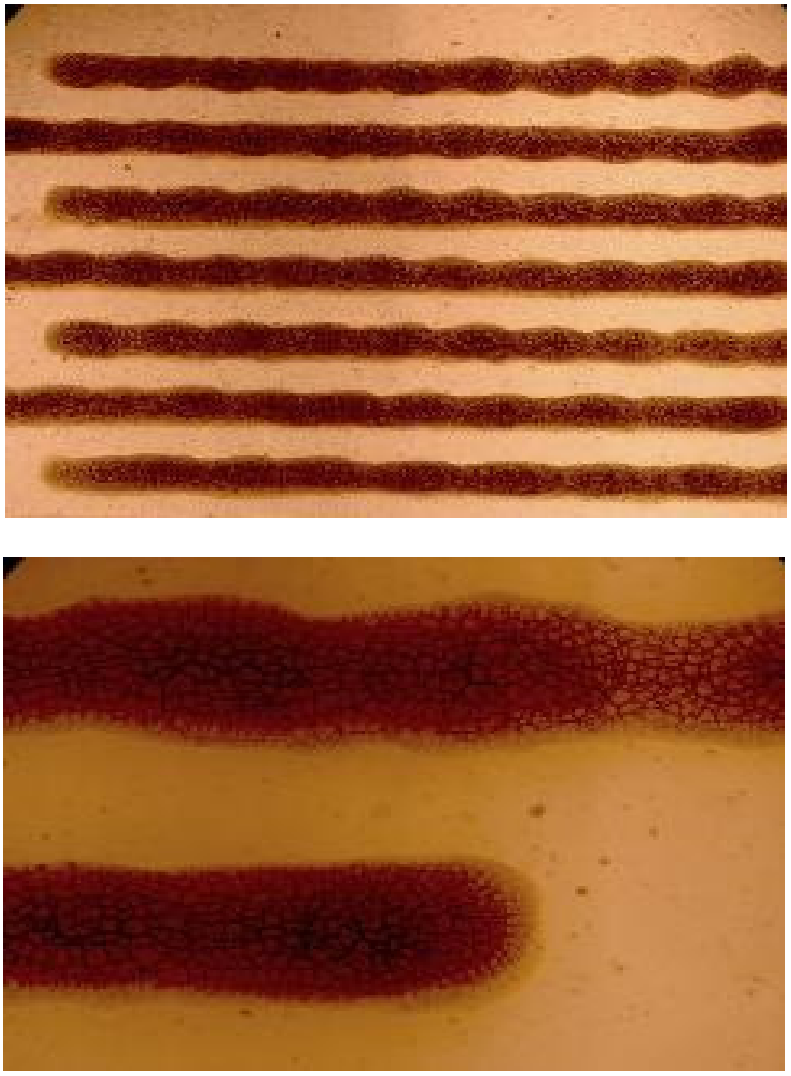

Figure 10 Images of printed GO lines. Droplets were ejected 80 μm from one another to pr oduce well connected lines.

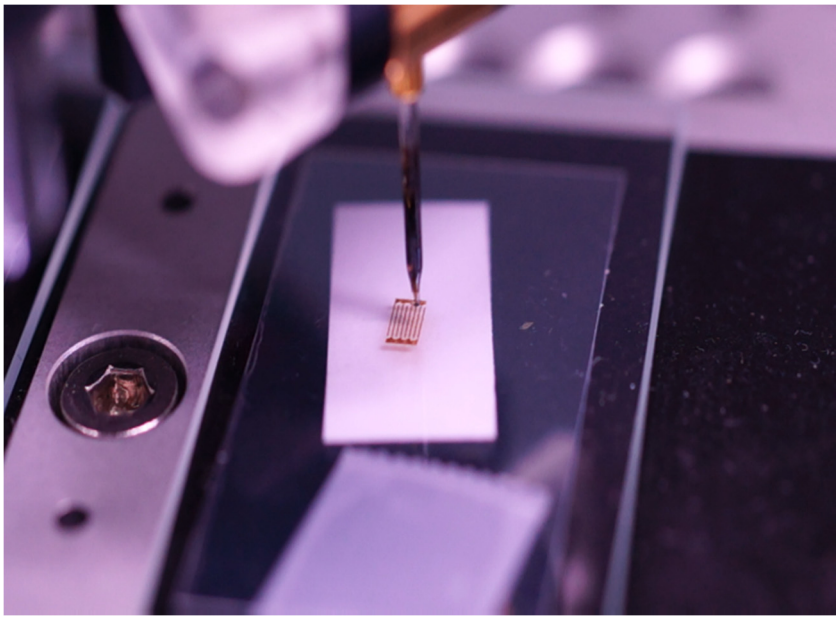

Figure 11 Direct printing of interdigitated pattern using programmable liquid dispenser.

3.4. Graphene oxide reduction

GO is a poor electrical conductor. During oxidation process, sp2 carbons are replaced by sp3 carbons which increase the band gap that diminishes the conductivity of the material. In fact, the conductivity of GO depends on the degree of oxidation. Therefore, a reduction treatment is necessary to recover the electrical properties of the pristine graphene through the removal of functionalities and restoration of aromatic graphene structure. Thermal[27], Photothermal [10, 28], plasma[29, 30], electrochemical[31] and chemical reduction[32, 33] methods have been demonstrated in many literatures as effective ways to reduce GO.

Photothermal reduction method offers advantages such as quick and chemical free reduction process, as well as operable in mild environment whereas high temperature condition is required in conventional thermal reduction. As reported by Kaner's group[34], graphene oxide could be reduced using laser source mounted in a commercial DVD laser scribe writer. GO solution was drop-casted on a PET film which was placed on the label side of a DVD disc, and was left in room environment to dry. The label side of the disc was faced downwards in the writer. rGO obtained using laser scribing is shown in Figure 12.

Controllable parameters of laser scribing includes track per inch (TPI), focus offset (FO) of the laser and laser power. TPI defines the radial distance between the circular tracks passed by the laser point. The 650 nm-wavelength coherent light source was operated at maximum power, 50 mW.

Optimization experiment of laser scribing number, TPI and laser FO were carried out. GO samples were laser scribed different time to investigate the corresponding reduction effect, which was indicated by the sheet resistance measurement using four point probe. GO was reduced in the first run. This was evident when initial GO sheet resistance decreased significantly from 10 MΩ/□ to about 250 Ω/□. However the value became stable and fluctuated around 180 Ω/□ after second time scribing.

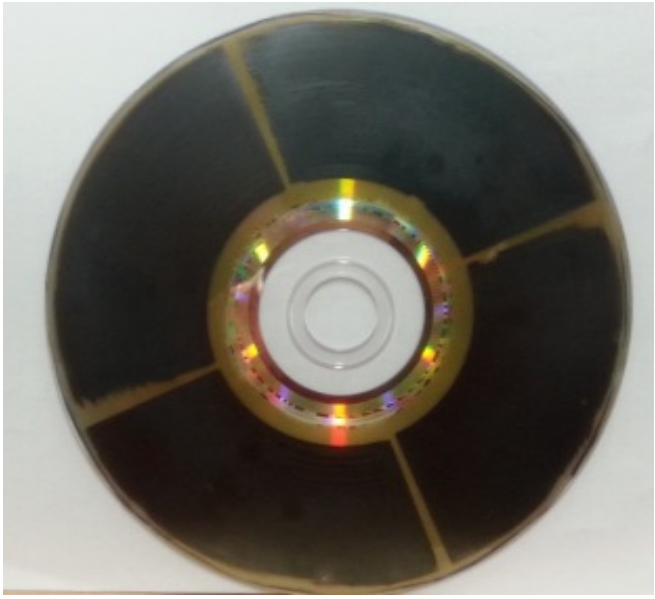

Figure 12 Laserscribing of GO on DVD disc. Brownish part is unreduced GO and dark part is reduced GO.

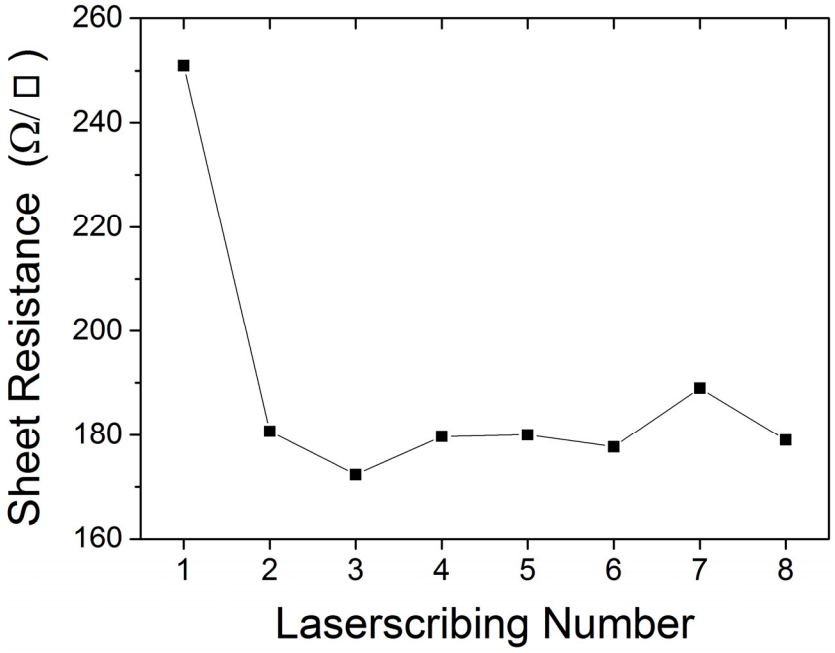

Graph 1 Effect of laser scribing repetition on rGO sheet resistance.

TPI was manipulated at different values: 600, 950, 1300, 1650 and 2000. The images of the laser scribed rGO are shown in Figure 13 from left to right. Sheet resistance of the 6-time-laser scribed rGO samples were measurement. The values dropped from 950 Ω/□ to 180 Ω/□ in the increase of TPI. This is straightforward that overall GO had higher degree of reduction when the laser paths became denser, meaning more area was exposed to laser source.

Figure 13 rGO produced from different TPI numbers: 600, 950, 1300, 1650 and 2000 respectively from left to right.

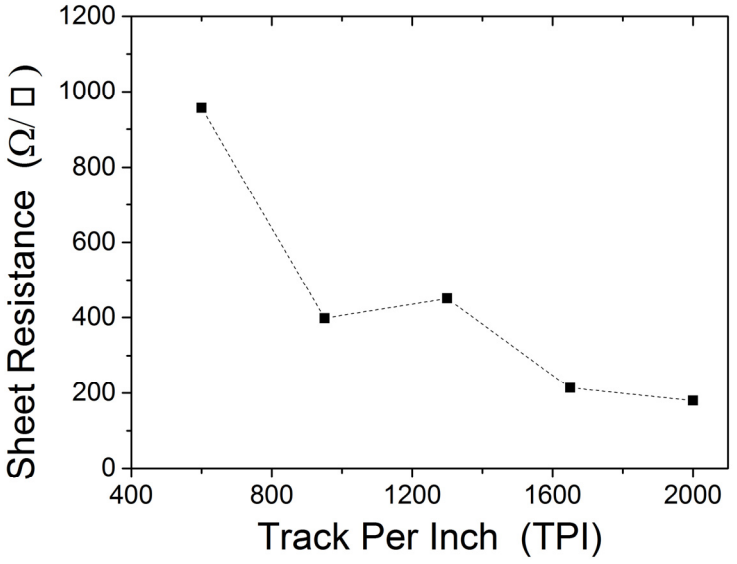

Graph 2 Effect of track per inch (TPI) on rGO sheet resistance. TPI defines density of laser scribing tracks or the width between the laser paths.

Laser focus offset at 0 is the default position of the DVD label surface. Since DVD disc was flipped upside down in the DVD writer, minus value referred to the position above the label surface where the GO coated PET was lying on. All samples were only single-time laser scribed. It was observed that laser scribing at -3 offset value gave the lowest sheet resistance.

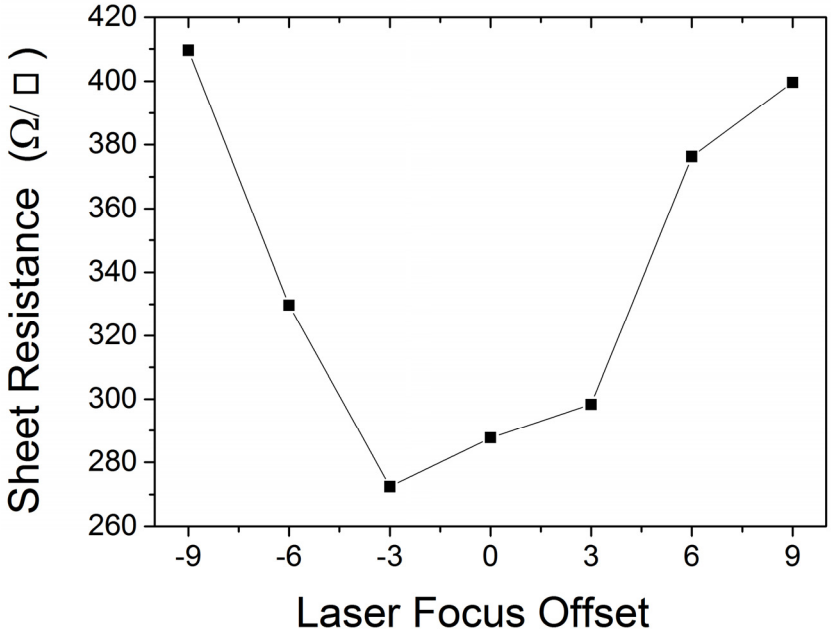

Graph 3 Effect of laser focus offset to rGO sheet resistance.

Photothermal reduction of GO was induced by laser scribing, accompanied by laser ablation that left crack lines on the rGO surface, which is visible in scanning electron microscopic image (Figure 14). rGO regions puffed up as a result of the exfoliation of the stacked graphene sheets (Figure 15). Nevertheless, the bottom layer of GO was found not properly reduced, which sheet resistance remained at high value, approximately 15 kΩ/□.

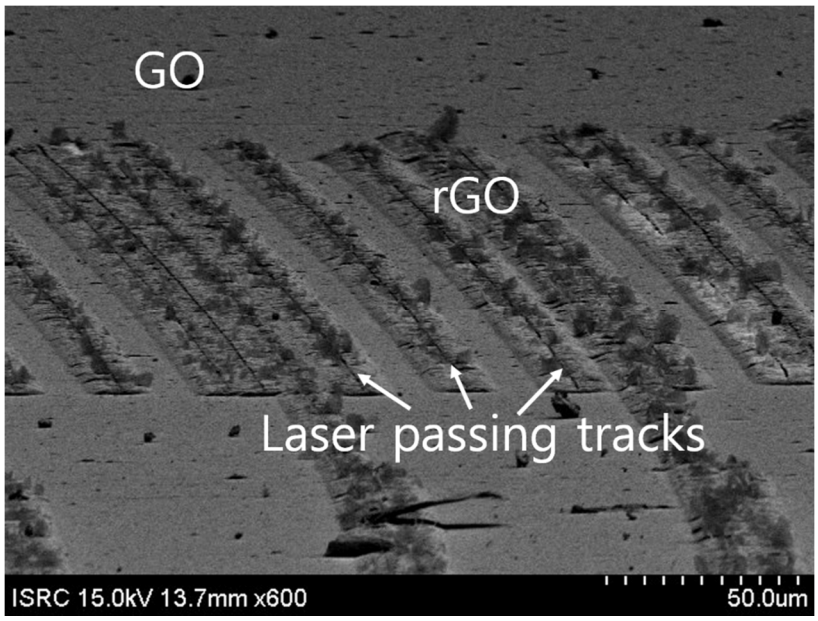

Figure 14 SEM image of laser passing tracks. rGO lines puffed up due to GO exfoliation.

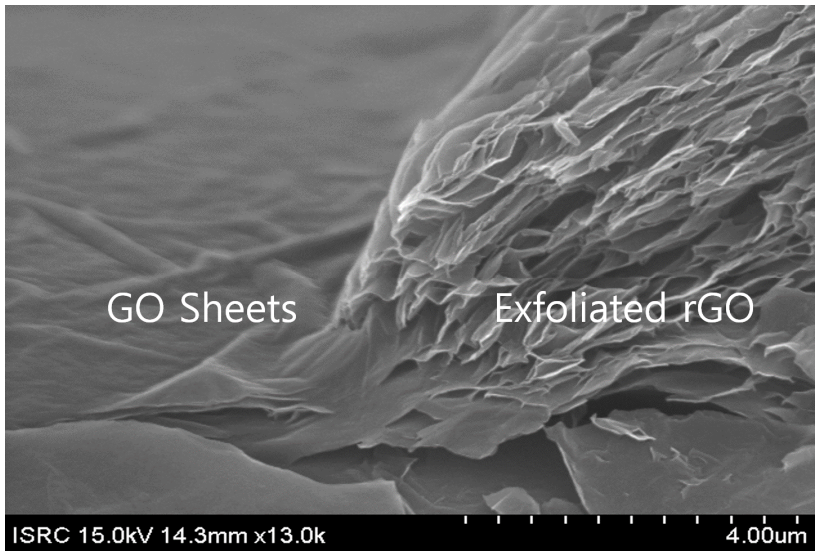

Figure 15 Magnification of rGO lines. Exfoliated rGO domain shows pores opened up by degassing process.

Alternatively, a camera flash accessory (Style RX 1200, Elinchrom, Switzerland) was also reported being used to photo-thermally reduce GO[26]. Reduction process is efficient from the aspect of processing time as energy transfers to GO instantaneously. As reported in the literature, energy provided by xenon flash far exceeds 70 mJ/cm^2, the heat energy needed to raise the temperature of 1 μm thick of GO from room temperature to 100˚C at which deoxygenating reactions take place.

Photothermal energy optimization is key to ensure the integrity of the printed structure after reduction. Flash energy was controlled at 1.50 J/cm^2 in GO reduction process. It was observed that GO remained un-reduced at low energy (0.79 J/cm^2), while actively reduced and broken into pieces at high energy level (6.36 J/cm^2).The moment energy was delivered to GO, an explosion sound effect of "pop" was audible, suggesting a rapid air expansion near the surface of GO due to degasing, which effectively exfoliates the stacked structure of graphite layer. The significant increase of total surface of rGO was attributed to the exfoliating mechanism that expanded the rGO thickness ten times after reduction process.

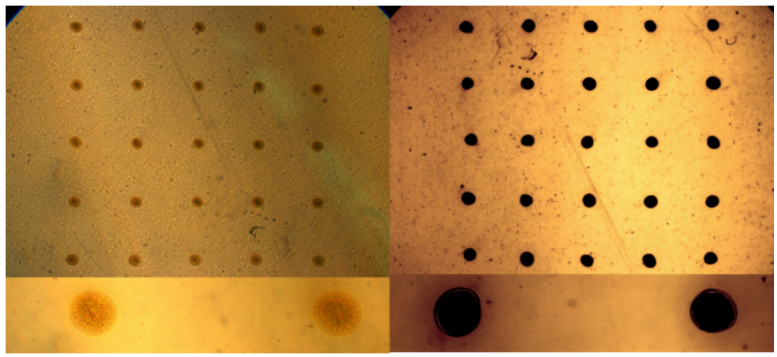

Figure 16 Photothermal reduction on GO spots using camera flash accessory.

Aside from observing color change from brown to black in Figure 16 and Figure 17, GO reduction was verified through Raman spectroscopy which is commonly used to characterize crystal structure, defect and disorder of a material. The measurement was conducted using LabRam Aramis (Horiba Jobin Yvon), 0.5 mW powered laser with 514 nm wavelength. The corresponding Raman spectrum is shown in Graph 4. D peak which represents the breathing mode of sp^2 rings[35], increased substantially after the reduction process, indicating the formation of sp^2 domain. The ratio of D peak and G peak (I_D/I_G) refers to the degree of disorder and inversely proportional to the size of sp^2 clusters. Increase of D/G peak ratio from 0.92 to 1.41 after photothermal reduction implied the formation of graphitic domain[36].

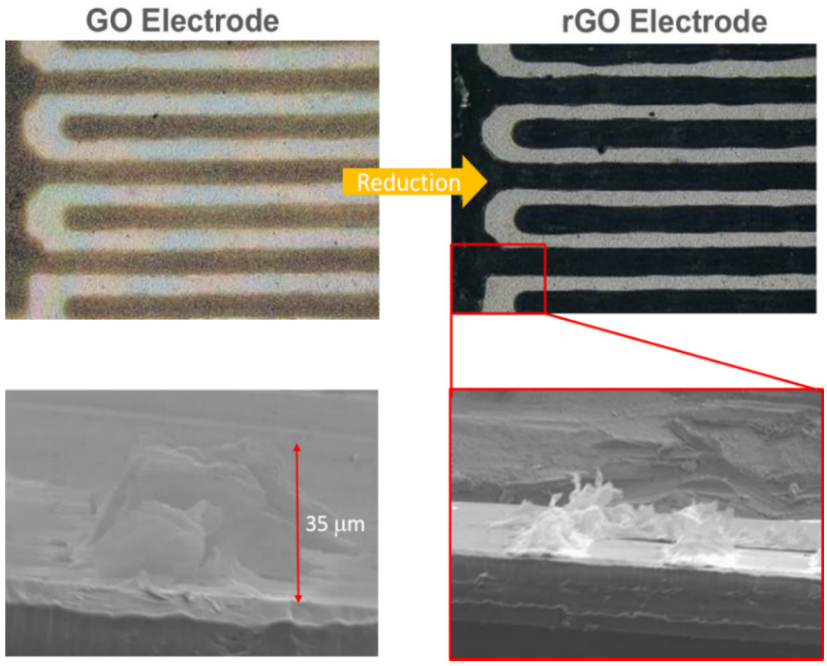

Figure 17 Flash reduction treatment on GO resulted in colour change and radical volume expansion.

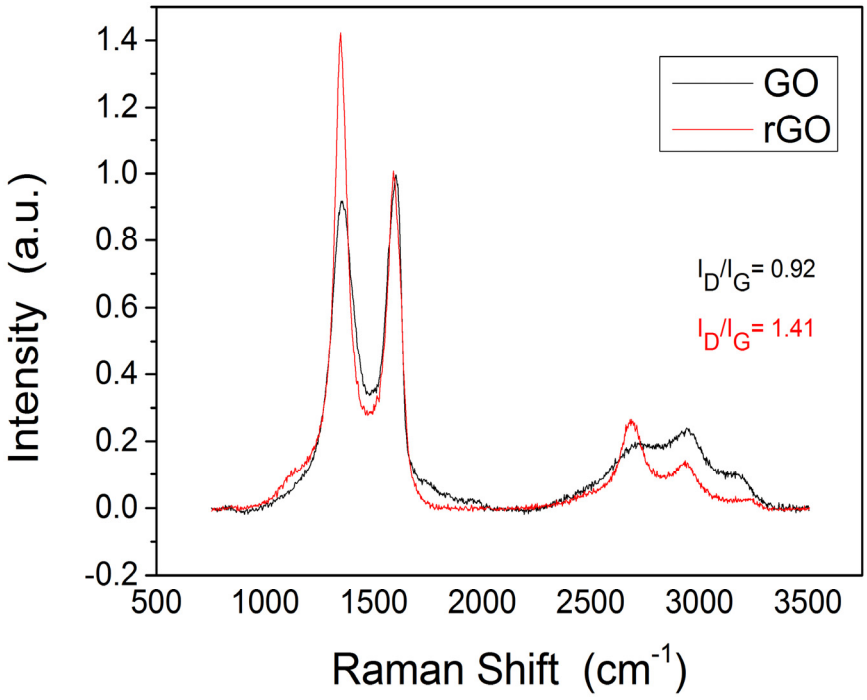

Graph 4 Raman spectroscopy of GO and rGO. Substantial increase of D peak after reduction treatment is observed. Increase of D/G peak ratio indicates the formation of graphitic domain.

3.5. Electrolyte

Poly(vinyl alcohol) (PVA)-H_2SO_4 polymer gel was used as electrolyte.[4] Gel electrolyte was made by dissolving PVA powder in water (1 g PVA : 10 g water) at 90 °C under constant stirring. The mixture was let cooling off after it became clear (Figure 18). Then 1 g of concentrated sulfuric acid was added to the mixture. The gel electrolyte was spread evenly on the printed electrode and was left in ambient environment for 5 hours. This was to ensure the electrolyte wet the rGO electrodes completely and evaporation of excess water from the gel. Gel electrolyte simplified the fabrication process because the device does not need additional packaging material for sealing liquid type electrolyte. After that, carbon paste was applied at the end of both electrodes as contact pads. The whole fabrication is schematically explained in Figure 20. Figure 19 shows the actual image of the device which is ready for measurement.

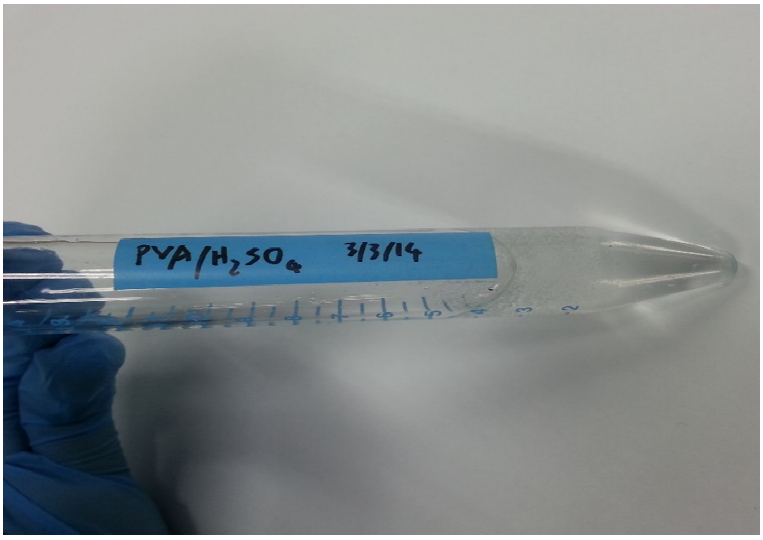

Figure 18 Transparent PVA-H2SO4 gel electrolyte.

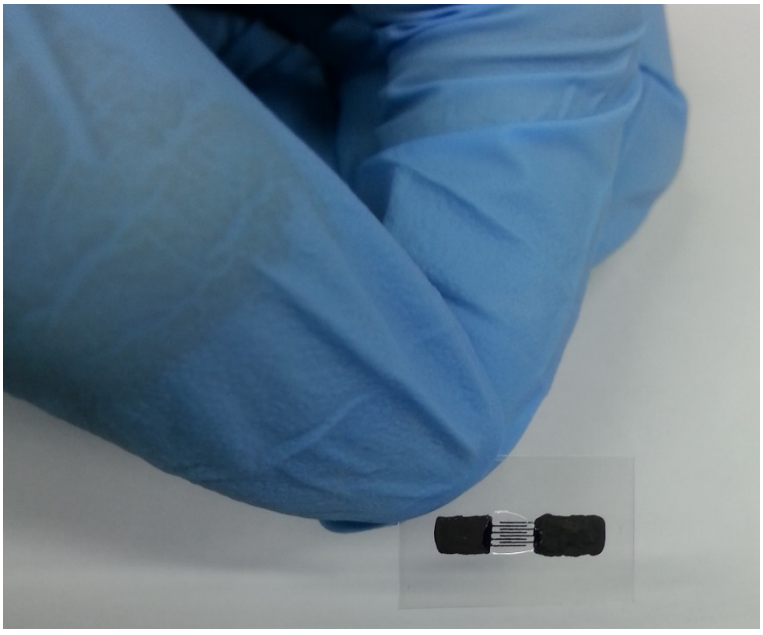

Figure 19 Image of fabricated supercapacitor. Gel electrolyte was coated on printed electrode and conductive carbon paste painted on both ends as contact pads.

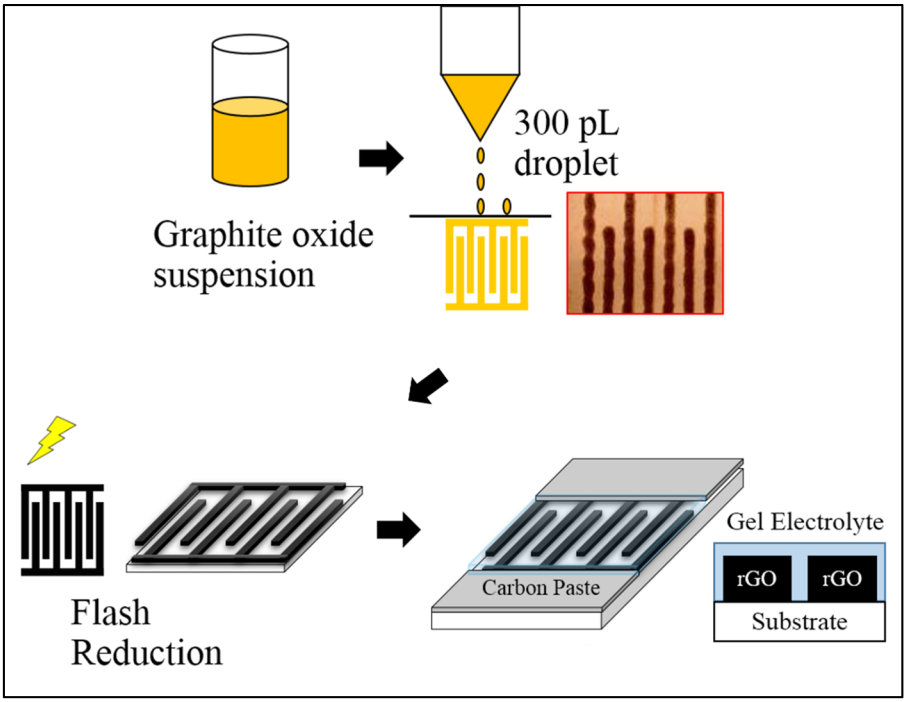

Figure 20 Fabrication flow of supercapacitor. Graphite oxide suspension is printed into interdigitated pattern using liquid dispenser. GO electrode is treated with flash radiation to induce reduction process. Lastly, gel electrolyte is coated on printed electrode and carbon paste is used to create contact pads at both ends.

4. Result

4.1. Cyclic voltammetry

Cyclic voltammetry (CV) is widely used to conduct electrochemical study on chemical compounds, reactions or an electrode materials. It is frequently used to characterize energy storage and conversion devices such as batteries, supercapacitors, and fuel cells. In a CV test, the electrical potential of working electrode is ramped linearly versus time within a potential window that sets the upper and lower limit of the potential sweep [37]. When the potential hits the upper or lower limit, the potential ramp will be reversed to make continuous cycles. Therefore, potential is swept forth and back in the potential window and the corresponding current is recorded, and then plotted against the potential, shown in cyclic voltammogram. The speed of the potential sweep is known as scan rate, expressed in the unit of V/s.

CV setup can be established either in two or three-electrode configuration depending on the purpose of study. Three-electrode configuration is prevalently used for fast screening and characterization of electrode materials. An additional reference electrode is used in three-electrode system, acting as a standard bar in the electrical potential measurement because it has stable and known potential. Various types of reference electrode are used, such as standard hydrogen electrode (SHE), saturated calomel electrode (SCE) and silver chloride electrode. On the

other hand, two-electrode configuration is inclined to whole cell performance evaluation under real operating conditions. CV was performed on the supercapacitor in two-electrode systems, at different scan rates: 25, 50, 100 and 250 mV/ to characterize the performance of the device (Graph 5). The potential window was limited within 1V to prevent the decomposition of the aqueous electrolyte.

The performance indices such as capacitance, energy and power densities were extracted from the cyclic voltammograms, and tabulated in Table 2 Performance indices of supercapacitor.. Capacitance can be measured as charge stored on the electrode divided by the potential window, expressed in equation below. Accumulated charge on the electrode surface can be estimated from the ratio of area integration of the cyclic voltammogram with respect to potential, and the scan rate. Therefore, the specific capacitance was calculated using

$$C_{sp} = \frac{\int IdE}{\Delta E.\upsilon.V},$$

where I, E, ΔE, ν and V are the electric current, potential, potential window, scan rate and volume, respectively. The energy density is given by

$$E_d = \frac{1}{2} C_{sp} \Delta E^2 .$$

The power density was calculated by dividing the energy density with the discharging duration of the device,

$$P_d = \frac{E_d}{\Delta t}$$

Rectangular cyclic voltammograms obtained indicates energy storage via electrical double layer mechanism. From the figure below, it is apparent that the magnitude of the current flowing between the working electrode and counter electrode was proportional to the scan rate. This phenomenon is attributed to the larger local electric field resulted by a rapid change of potential on the electrode surface[38]. At low scan rate, CV curve was more rectangular, implying good capacitive behavior. However, the rectangular shape gradually distorted at increasing scan rates, as "hump" starts to become more obvious at the corner. The appearance of the "hump" could be interpreted as capacitance drop because of the shrink of voltammogram area. The capacitance drop at higher scan rates is due to larger resistance to ionic currents resulted by fast potential sweeping, which is common in electrical double layer capacitor (EDLC) based on porous carbon material. This phenomenon was discussed in several literatures [38, 39], regarding the saturation of surface area occupied by the ions before reaching the maximum electrical potential. At low scan rates, electrodes are more accessible by the ions due to the deformation of the pore which is similar to intercalation process, thus resulting in higher capacitance at lower scan rate.

A Ragone plot (Graph 6) is used to compare the performance of various energy storing devices. Energy densities are plotted against power densities at increasing scan rates. From the plot, all kinds of supercapacitor position

between electrolytic capacitor and thin film battery. Printed rGO supercapacitor attained similar energy densities as laser scribed rGO supercapacitor, but the power densities fell approximately one order lower than its counterpart. The reason behind this is due to the absence of current collector that caused high impedance in printed rGO supercapacitor. The impedance of the device is discussed in more detail in following section.

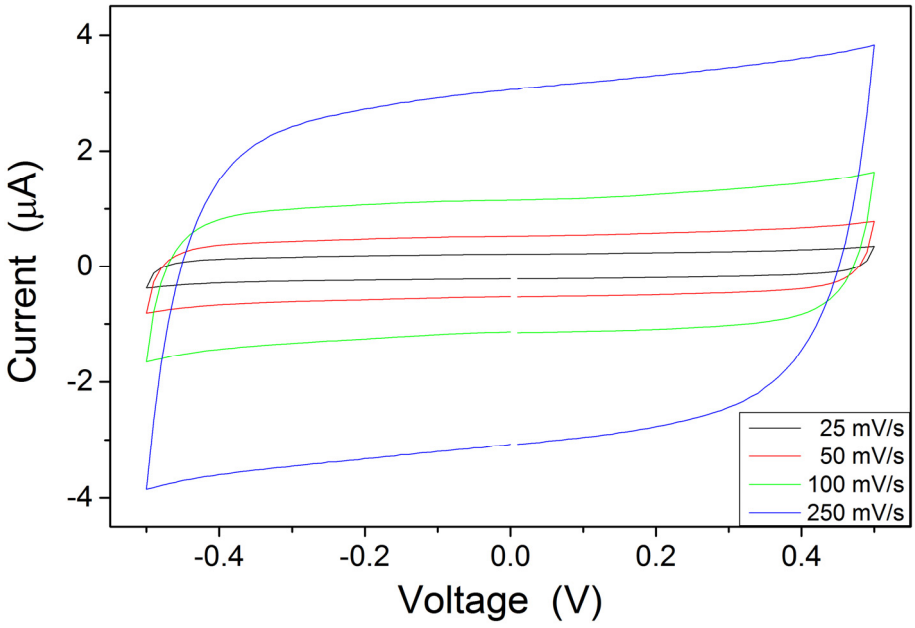

Graph 5 Cyclic voltammetry measurement at different scan rates: 25, 50, 100 and 250 mV/s.

Table 2 Performance indices of supercapacitor.

CV Area (AV)	Potential Window (V)	Scan Rate (V/s)	Active Area (cm^2)	Thickness (μm)	Discharging Time (s)	Specific Capacitance (F/cm^3)	Energy Density (mWh/cm^3)	Power Density (Wh/cm^3)
3.813E-07	1	0.01	0.033075	10	100	1.152	0.160	0.0058
9.150E-07	1	0.025	0.033075	10	40	1.106	0.154	0.0138
1.516E-06	1	0.05	0.033075	10	20	0.917	0.127	0.0229
2.835E-06	1	0.1	0.033075	10	10	0.857	0.119	0.0428
5.418E-06	1	0.25	0.033075	10	4	0.655	0.091	0.0819
9.687E-06	1	0.5	0.033075	10	2	0.586	0.081	0.1464
1.293E-05	1	1	0.033075	10	1	0.391	0.054	0.1955

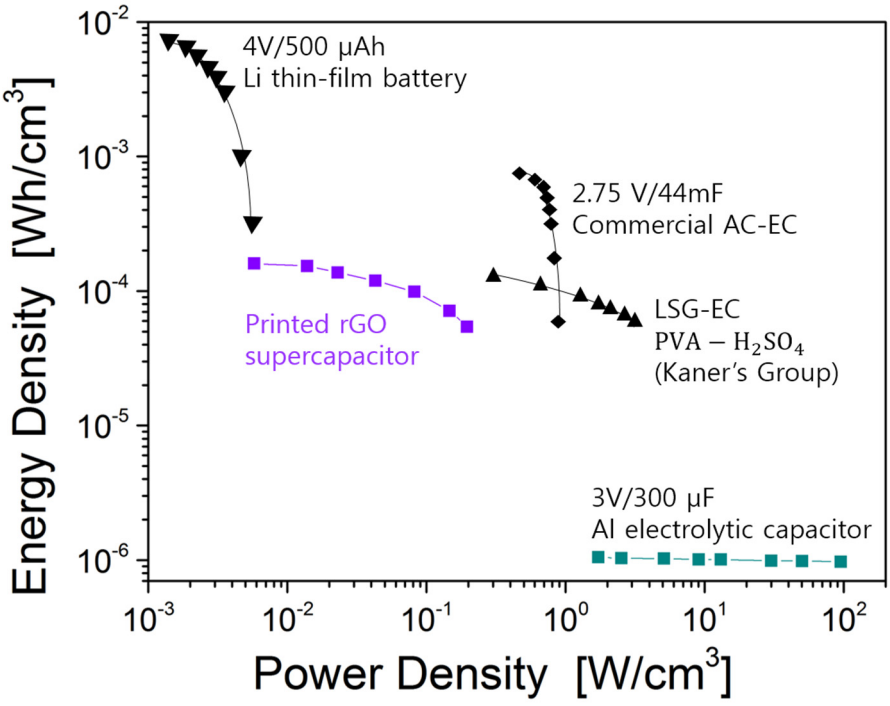

Graph 6 Ragone Plot. Performance of printed rGO supercapacitor is compared with other devices.[10]

4.2. Charging-discharging test

The behavior of a supercapacitor can be studied by charging and discharging the device. Charging-discharging can be carried either at constant electrical potential or constant current. Approach discussed in this thesis is restricted to the constant current or galvanostatic charging-discharging test. The equivalent circuits of supercapacitor are illustrated in Figure 21, which includes the equivalent series resistance R_S, electrical double layer capacitance C_{DL} and Faradaic resistance or leakage resistance R_F. V_{SC} represents the potential of the device while V_{DL} is defined as the potential across double layer.

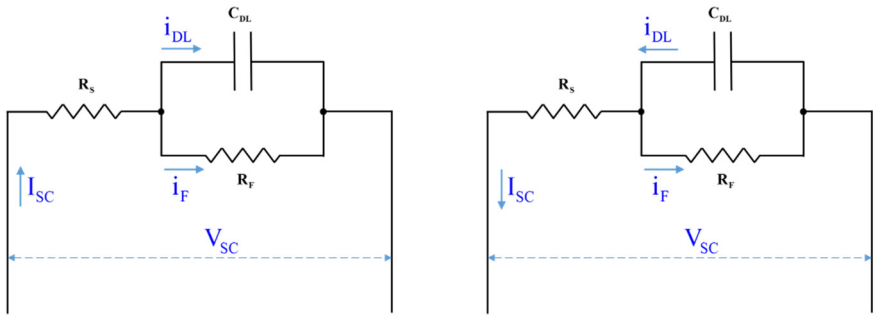

Figure 21 Equivalent circuits during charging and discharging of supercapacitors.

Prior to charging, the supercapacitor is considered to be zero charged and so zero potential, $V_{DL} = 0$. Therefore, when charging process starts at $t = 0$, the potential profile of the supercapacitor can be expressed as [40]

$$C_{DL}\frac{dV_{DL}}{dt} + \frac{V_{DL}}{R_F} = I_{SC}$$

By solving the differential equation with initial condition such that at $t = 0$ $V_{DL} = 0$, one can obtain

$$V_{DL} = I_{SC}R_F(1 - \exp(-\frac{t}{R_F C_{DL}}))$$

Since $V_{SC} = V_{DL} + I_{SC}R_S$, the potential of the device during charging process is

$$V_{SC} = I_{SC}R_S + I_{SC}R_F(1 - \exp(-\frac{t}{R_F C_{DL}}))$$

After fully charged, the maximum value of the electrical potential across the double layer is denoted as $V_{Max\,DL}$.The discharging process can be expressed by

$$\frac{1}{C_{DL}}\int i_{DL}dt + i_{DL}R_F - (V_{Max\,DL} + I_{SC}R_F) = 0$$

As $V_{DL} = V_{Max\,DL} - \frac{1}{C_{DL}}\int i_{DL}dt$,

$$V_{DL} = V_{Max\,DL} - (V_{Max\,DL} + I_{SC}R_F)[1 - \exp(-\frac{t}{R_F C_{DL}})]$$

During discharging, $V_{DL} = V_{SC} + i_{SC}R_S$. Therefore, the potential profile of the device can be expressed as

$$V_{SC} = V_{Max\,DL} - (V_{Max\,DL} + I_{SC}R_F)[1 - \exp(-\frac{t}{R_F C_{DL}})] - i_{SC}R_S$$

The charging-discharging tests were carried out at constant current of different magnitudes: 1, 3 and 5 μA (Graph 7). The triangular curves imply double layer capacitive energy storage mechanism. The potential drop at the beginning of the discharging process is visible, due to the equivalent series resistance occurs in the operation.

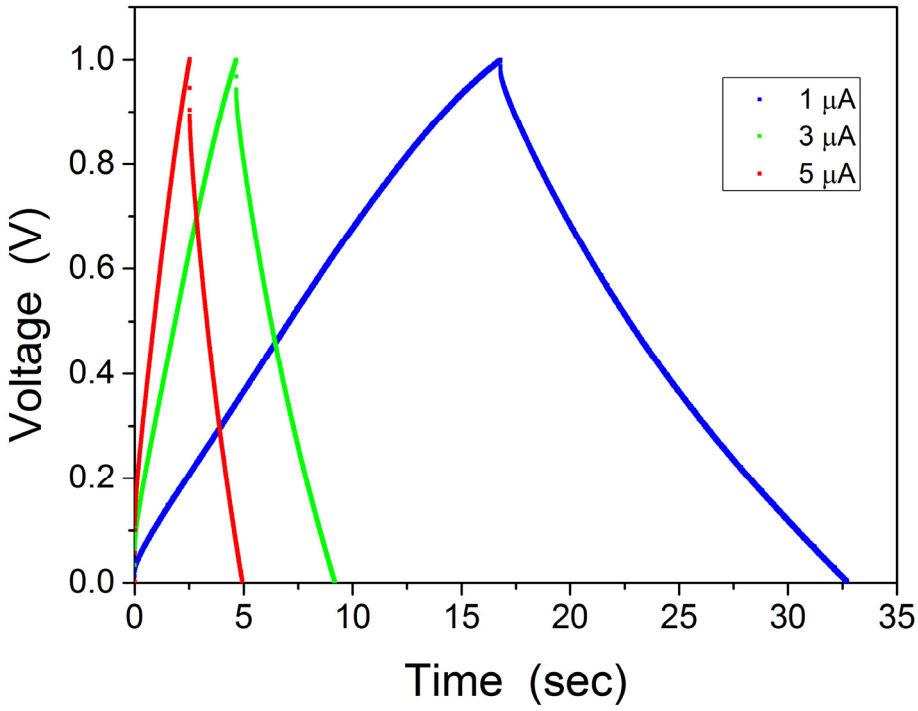

Graph 7 Galvanostatic charging-discharging test. 1, 3 and 5µA constant current was used to charge the device.

4.3. Electrochemical impedance spectroscopy

Electrochemical impedance spectroscopy (EIS) is a more sophisticated technique to characterize the performance of the supercapacitors. EIS is able to separately evaluate multiple components such as electric double layer capacitance, equivalent series resistance (ESR) and Faradaic leakage resistance simultaneously. Impedance can be explained as resistance which impedes the flow of electrical current, but additionally includes the information of frequency dependency. Impedance measurement is carried out in such way that an alternating voltage ($V_t = V_o \cos\omega t$) is inserted to a system and the resultant current ($I_t = I_o \cos(\omega t - \Phi)$) is monitored. Thus, impedance, Z is given as V_t/I_t. Electrochemical reaction on electrode-electrolyte interface can be represented through an equivalent circuit model, in which a capacitor and a resistance are connected in parallel as shown in figure below. The impedance of a capacitor is given as $Z_c = 1/j\omega C$ while a resistor's is $Z_R = R$. R_S represents the ESR of the circuit that includes the internal resistance of the cell as well as the solution resistance. R_F is the Faradaic leakage resistance or known as charge transfer resistance taking place at the electrode-electrolyte interface. R_F impedes the chemical reactions at the interface by hindering electron transfer from the electrodes to the reactive species on the vicinity of the electrode. Electrical double layer capacitance is denoted as C_{DL}, is the capacitance arises from the formation of ion layer on the electrode to balance the charge of the electrode.

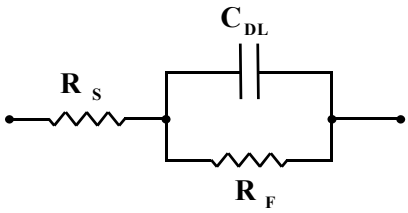

$$\frac{1}{Z_{Total}} = \frac{1}{Z_C} + \frac{1}{Z_R}$$

After re-arranging the terms, the impedance can be expressed in real and imaginary parts, such that

$$(Z^{"})^2 + (Z^{'} - R/2)^2 = (R/2)^2 .$$

The real part of the impedance corresponds to the resistance components while the frequency dependent imaginary part reveals capacitance information. Therefore, the simple parallel RC circuit can be plotted in complex-plane impedance plot as following.

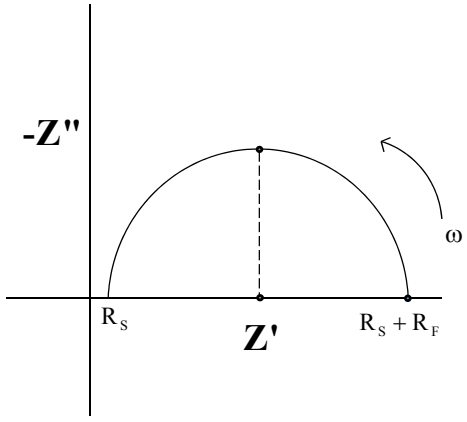

Figure 22 Nyquist plot of electrical double layer.

Impedance measurement was taken from 100 kHz to 0.1 Hz, with input voltage of 5 mV amplitude. The impedance spectroscopy is shown in Graph 8. The ESR of supercapacitor can be estimated from the intercept of x-axis, which was 138 Ω. There are several reasons that gave rise to this fairly high

ESR value. Firstly, the removal of current collectors effectively simplified the structure of the device, but resulted in higher resistance to the flow of charge because electrons had to travel along the electrodes instead of highly conductive metal material. Secondly, the reduction of GO was imperfect, which still contained functional groups after photothermal reduction process. The carbon-oxygen (CO) ratio of rGO was quantitatively determined by X-ray photoelectron spectroscopy [41]. The remaining impurities affected the electrical properties of the electrode material, ultimately leading to high ESR index.

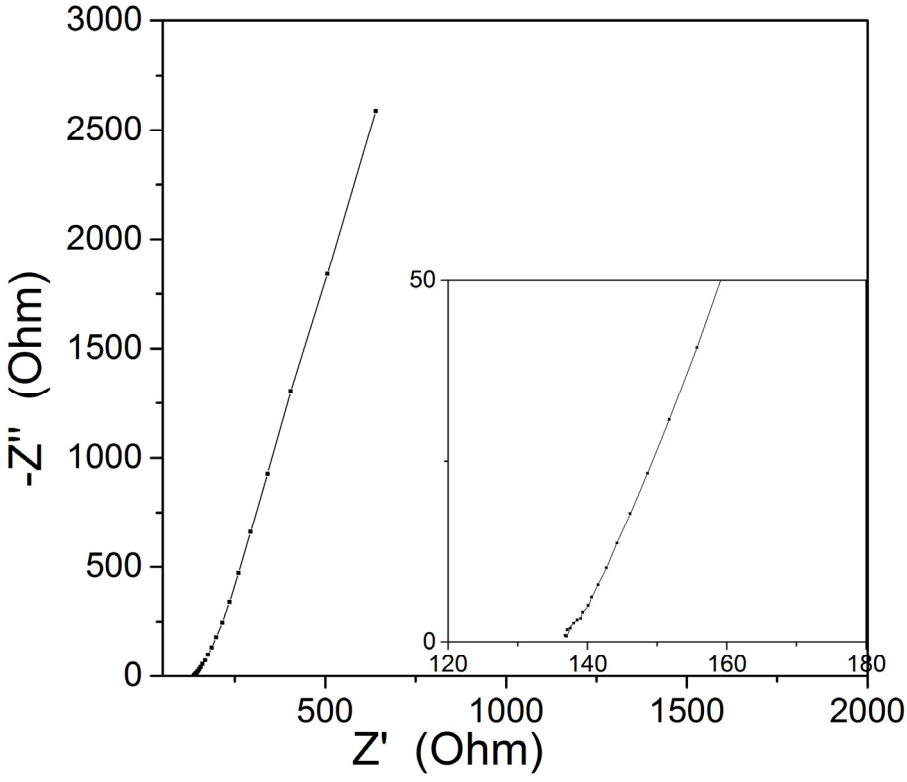

Graph 8 Electrochemical impedance spectroscopy (EIS) of supercapacitor. Frequency was scanned from 100 kHz to 1 Hz. The x-axis intercept revealed the equivalent series resistance of the device, 138Ω.

4.4. Capacitance retention test

It is crucial to inspect the cyclability of supercapacitor because excellent cycle life is one of supercapacitor's identity. Capacitance retention test was performed on the device using cyclic voltammetry at 100 mV/s for 2000 continuous cycles. The fabricated supercapacitor could retain about 89 % of the original capacitance after 2000 cycles.

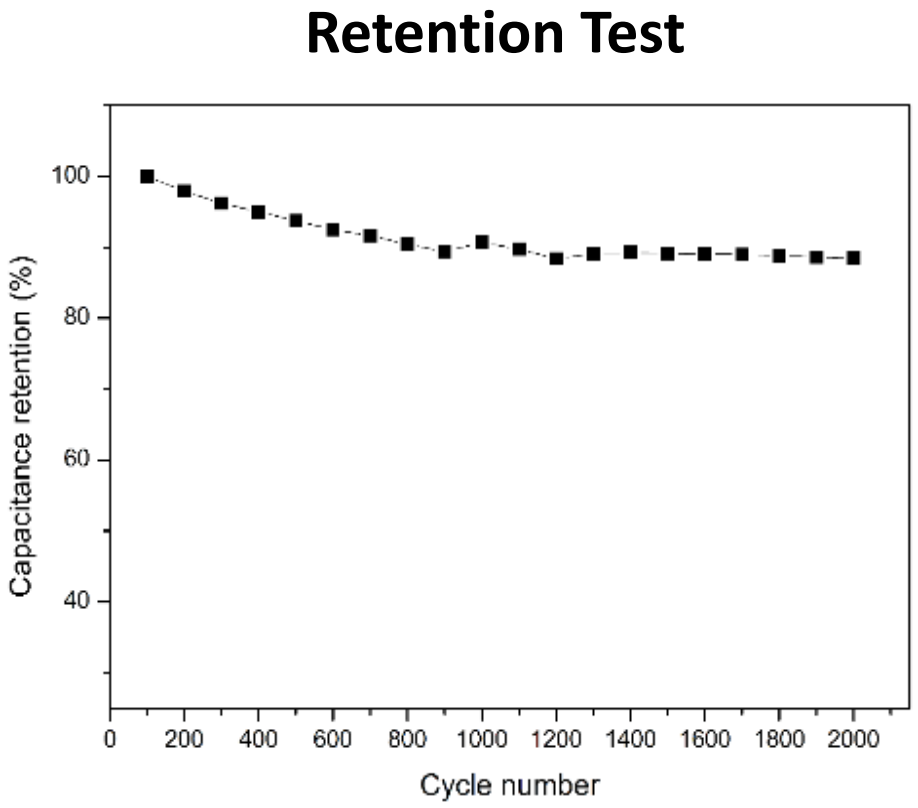

Graph 9 Capacitance retention of supercapacitor. 2000 cycles of CV test at 100 mV/s were conducted on the device.

5. Conclusion

The research on supercapacitors are actively taking place because of the increasing demand of energy storage systems for electronic devices. Hence, this thesis is dedicated to explore alternative route of fabricating reduced graphene oxide based supercapacitor. Direct printing approach proposed in this work offers many advantages. Firstly, printing of graphene oxide solution enables facile graphene oxide patterning process that whole procedures can be completed in ambient condition, even without MEMS fabrication. Secondly, GO patterns can be realized on various substrate materials through direct printing to serve versatile applications. Moreover, the combination of graphene oxide printing and reduction simplified the architecture of supercapacitors that eliminate current collectors and separator components.

In addition, electrochemical methods were used to characterize the performance of fabricated supercapacitors. Important indices such as specific capacitance, energy and power densities were determined: $1.152\ \mathrm{F/cm^3}$, $0.16\ \mathrm{mWh/cm^3}$ and $0.1955\ \mathrm{Wh/cm^3}$ respectively. It was found that the performance of supercapacitor was inferior in comparison with current literature results due to several factors, which should be addressed separately in detail. Nevertheless, the fabrication process demonstrated in this thesis is valuable as it serves as a starting point that shows possibilities in future development.

References

1. P.Simon, J.R.M.a., *The Chalkboard - Fundamentals of Electrochemical Capacitor Design and Operation.* The Electrochemical Society's Interface, 2008. **17**(1): p. 31-32.

2. Bo, S.-H., et al., *Degradation and (de)lithiation processes in the high capacity battery material LiFeBO3.* Journal of Materials Chemistry, 2012. **22**(18): p. 8799.

3. Pech, D., et al., *Ultrahigh-power micrometre-sized supercapacitors based on onion-like carbon.* Nat Nanotechnol, 2010. **5**(9): p. 651-4.

4. El-Kady, M.F., et al., *Laser scribing of high-performance and flexible graphene-based electrochemical capacitors.* Science, 2012. **335**(6074): p. 1326-30.

5. Jason P Lee, Product How-to: Extending battery life in transportation and mobile applications with supercapacitors, 11 December 2013, EDN Network, http://www.edn.com/design/power-management/4425935/3/Product-How-to--Extending-battery-life-in-transportation-and-mobile-applications-with-supercapacitors

6. Matsunaga, T., et al., *Molecular analysis of magnetotactic bacteria and development of functional bacterial magnetic particles for nano-biotechnology.* Trends in Biotechnology, 2007. **25**(4): p. 182-188.

7. Stoller, M.D., et al., *Graphene-based ultracapacitors.* Nano Lett, 2008. **8**(10): p. 3498-502.

8. John Chmiola, C.L., Pierre-Louis Taberna, Patrice Simon, Yury Gogotsi, *Monolithic Carbide Derived Carbon Films for Micro-Supercapacitors.* Science, 2010. **328**(5977): p. 480-483.

9. Gao, W., et al., *Direct laser writing of micro-supercapacitors on hydrated graphite oxide films.* Nat Nanotechnol, 2011. **6**(8): p. 496-500.

10. El-Kady, M.F. and R.B. Kaner, *Scalable fabrication of high-power graphene micro-supercapacitors for flexible and on-chip energy storage.* Nat Commun, 2013. **4**: p. 1475.

11. Xue, M., et al., *Structure-Based Enhanced Capacitance: In Situ Growth of Highly Ordered Polyaniline Nanorods on Reduced Graphene Oxide Patterns.* Advanced Functional Materials, 2012. **22**(6): p. 1284-1290.

12. Xu, Y., et al., *Inkjet-printed energy storage device using graphene/polyaniline inks.* Journal of Power Sources, 2014. **248**: p. 483-488.

13. Pauling, L., *<The size of ions and the structure of ionic crystals.pdf>*. J. Am. Chem. Soc., 1927. **49**: p. 771.

14. Conway, B.E., *Electrochemical Supercapacitors: Scientific Fundamentals and Technological Applications*. 1999: Kluwer Academic/Plenum Publishers.

15. M. Endo, T.T., Y.J. Kim, K. Koshiba and K. Ishii, *High power EDLC from operating principle to pore size control in advanced activated carbons.* Carbon Science, 2001. **1**(3 & 4).

16. A.M. Bond, R.G.C., D.A. Fiedler, G. Inzelt, H. Kahlert, S. Komorsky-Lovric, H. Lohse, M. Lovric, F. Marken, A. Neudeck, U. Retter, F. Scholz, Z. Stojek, <*Electroanalytical Methods : Guides to Experiments and Applications*>. Second Edition ed, ed. D.F. Scholz. 2009: Springer. 359.

17. Wikipedia, Double layer(interfacial) http://en.wikipedia.org/wiki/Double_layer_(interfacial)#mediaviewer/File:EDLC-Potentialdistribution.png

18. Schon, T.B., P.M. DiCarmine, and D.S. Seferos, *Polyfullerene Electrodes for High Power Supercapacitors.* Advanced Energy Materials, 2014. **4**(7): p. n/a-n/a.

19. Cheng, Q., et al., *Graphene and carbon nanotube composite electrodes for supercapacitors with ultra-high energy density.* Phys Chem Chem Phys, 2011. **13**(39): p. 17615-24.

20. Zhu, Y., et al., *Carbon-based supercapacitors produced by activation of graphene.* Science, 2011. **332**(6037): p. 1537-41.

21. Katsnelson, M.I., *Graphene: carbon in two dimensions.* Materials Today, 2007. **10**(1-2): p. 20-27.

22. Huang, Y., J. Liang, and Y. Chen, *An overview of the applications of graphene-based materials in supercapacitors.* Small, 2012. **8**(12): p. 1805-34.

23. Xiong, G., et al., *A Review of Graphene-Based Electrochemical Microsupercapacitors.* Electroanalysis, 2014. **26**(1): p. 30-51.

24. Yoo, J.J., et al., *Ultrathin planar graphene supercapacitors.* Nano Lett, 2011. **11**(4): p. 1423-7.

25. Scienion, http://www.scienion.de

26. Laura J. Cote, R.C.-S., and Jiaxing Huang, *Flash Reduction and Patterning of Graphite Oxide and Its Polymer Composite.* Journal of the American Chemical Society, 2009. **131**: p. 11027-11032.

27. Chen, W., L. Yan, and P.R. Bangal, *Preparation of graphene by the rapid and mild thermal reduction of graphene oxide induced by microwaves.* Carbon, 2010. **48**(4): p. 1146-1152.

28. Zhang, Y., et al., *Direct imprinting of microcircuits on graphene oxides*

film by femtosecond laser reduction. Nano Today, 2010. **5**(1): p. 15-20.

29. Kumar, N.A., et al., *Plasma-assisted simultaneous reduction and nitrogen doping of graphene oxide nanosheets.* Journal of Materials Chemistry A, 2013. **1**(14): p. 4431.

30. Lee, S.W., et al., *Plasma-Assisted Reduction of Graphene Oxide at Low Temperature and Atmospheric Pressure for Flexible Conductor Applications.* The Journal of Physical Chemistry Letters, 2012. **3**(6): p. 772-777.

31. Yang, J. and S. Gunasekaran, *Electrochemically reduced graphene oxide sheets for use in high performance supercapacitors.* Carbon, 2013. **51**: p. 36-44.

32. Some, S., et al., *High-quality reduced graphene oxide by a dual-function chemical reduction and healing process.* Sci Rep, 2013. **3**: p. 1929.

33. Chen, W. and L. Yan, *In situ self-assembly of mild chemical reduction graphene for three-dimensional architectures.* Nanoscale, 2011. **3**(8): p. 3132-7.

34. V.Strong, S.D., etc., , *Patterning and Electronic Tuning of Laser Scribed Graphene for Flexible All-Carbon Devices.* American Chemical Society, 2012. **6**(2).

35. Che, J., L. Shen, and Y. Xiao, *A new approach to fabricate graphene nanosheets in organic medium: combination of reduction and dispersion.* Journal of Materials Chemistry, 2010. **20**(9): p. 1722.

36. Guo, Y., et al., *One pot preparation of reduced graphene oxide (RGO) or Au (Ag) nanoparticle-RGO hybrids using chitosan as a reducing and stabilizing agent and their use in methanol electrooxidation.* Carbon, 2012. **50**(7): p. 2513-2523.

37. Majumdar, S.R.a.P., *Fuel Cells: Principles, Design, and Analysis*. 2014: CRC Press.

38. Wang, H. and L. Pilon, *Physical interpretation of cyclic voltammetry for measuring electric double layer capacitances.* Electrochimica Acta, 2012. **64**: p. 130-139.

39. Mysyk, R., E. Raymundo-Piñero, and F. Béguin, *Saturation of subnanometer pores in an electric double-layer capacitor.* Electrochemistry Communications, 2009. **11**(3): p. 554-556.

40. Ban, S., et al., *Charging and discharging electrochemical supercapacitors in the presence of both parallel leakage process and electrochemical decomposition of solvent.* Electrochimica Acta, 2013. **90**: p. 542-549.

41. Jung, H., et al., *Direct printing and reduction of graphite oxide for flexible supercapacitors.* Applied Physics Letters, 2014. **105**(5): p. 053902.